JOURNAL OF GEOPHYSICAL RESEARCH, VOL. 104, NO. C1, PAGES 1377–1392, JANUARY 15, 1999

Isopycnic modeling of the North Atlantic heat budget

Ian Jones

Environment Centre, Leeds University, Leeds, England, United Kingdom

Harry Leach

Oceanography Laboratories, Liverpool University, Liverpool, England, United Kingdom

Abstract. A 2° resolution version of the Miami Isopycnic Coordinate Ocean Model is used within an idealized basin to examine the ocean heat budget. Simplified seasonal wind stress and thermohaline forcing, based on observational data of the North Atlantic, are used to drive the model. Following a 30-year spin-up, the model reaches a state of little annual heat content change, at which point a detailed study of the heat budget is performed. The heat budget is split into the components of surface forcing, diffusion, Ekman pumping, Ekman transport, and non-Ekman advection. Both annual and seasonal results are obtained. Analysis of the heat budget reveals different annual balances to exist in different ocean regions. In the subpolar gyre the principal balance is between cooling caused by surface fluxes and warming due to geostrophic advection. However, in the subtropical gyre, where net surface fluxes are small, Ekman pumping balances geostrophic advection. As such, the Ekman pumping is seen to be important for supplying the necessary heat for subduction to take place. An investigation of the Ekman compensatory flow is undertaken. It is shown that the exact temperature and, consequently, the depth of this flow are important for determining the Ekman heat content change. The results here tentatively suggest this depth to be in the upper thermocline. Subduction rates are calculated and shown to be reasonable. The seasonal heat budget is dominated everywhere by surface fluxes. All other terms have negligible seasonal cycles, except for the Ekman terms, which exhibit a limited seasonal variation. In doing so the Ekman terms are seen to control the seasonal cycle of the transport of heat. This is due to their dependency on not only the time variation in wind stress but also the degree of stratification of the upper ocean.

1. Introduction

In an investigation of the heat balances that exist within the climate system the ocean is of special interest because the high specific heat capacity of water, together with its great density, lead to the heat content of the ocean far exceeding that of the atmosphere. The North Atlantic heat budget is of particular interest, as there is an exchange of cold, deep waters formed on its northern borders for warmer surface waters from the south. This exchange is thought to increase the air temperature over Europe by several degrees above that which would be achieved if the exchange were not taking place [*Rind et al.*, 1986].

At high latitudes, extreme thermal forcing causes subduction and consequent water mass formation to occur at localized deep convection sites. Mechanical forcing brings about more widespread subduction into the thermocline either through the downward pumping of water or through lateral motion across the sloping base of the winter mixed layer. In the North Atlantic, mixed layer water is subducted into the thermocline across the subtropical gyre, where water columns are moving southward under the influence of the geostrophic flow. This lateral subduction requires a supply of buoyancy to the mixed layer [*Nurser and Marshall*, 1991]. The supply of heat that induces the necessary shoaling of the mixed layer is therefore of considerable interest. It has been proposed [*Marshall et al.*, 1993; *Marshall and Marshall*, 1995] that Ekman pumping significantly increases the available heat, above and beyond that provided by the air-sea flux. The proportion of this heating being attributable to different processes is pertinent to both understanding the subduction as it is now and for understanding any future changes to the system.

The seasonal heat balance is also of interest, with some debate over the relative importance of the atmospheric heat fluxes compared to the advective contribution of heat to a water column. *Gill and Niiler* [1973] argued that the seasonal balance should be between

Paper number 1998JC90043.
0148-0227/99/1998JC900043$09.00

surface heating and heat storage, and this result was reproduced by *Sarmiento* [1986] using a z coordinate model and was in agreement with the observations of *McCulloch* [1995]. However, *Lamb and Bunker* [1982] showed observational data where the advective effects, calculated as a residual, were equally as large. Earlier, a similar result had been produced by *Bathén* [1971]. Advective effects themselves may be subdivided into those brought about by the geostrophic flow and those taking place as a result of the Ekman processes induced by the wind stress field.

It is the purpose of this paper to further clarify the role of the Ekman processes in causing subduction to occur and to add to the existing body of evidence covering both the annual and seasonal heat balances that exist in the North Atlantic. This is accomplished by modeling an idealized ocean basin and analyzing the heat balances formed. The model used is an isopycnic one [*Bleck et al.*, 1992], this formulation avoiding the spurious diapycnic mixing to which most depth coordinate models are prone and thus more accurately mimicking the tendency of water masses to move within pseudo-material density interfaces. A coarse resolution version is used with zonal surface forcing in order to reduce computer time and simplify the experiment. This avoids complications caused by varied topography and so allows for an easier understanding of the results, but does not capture meso- or smaller-scale motions such as eddy processes.

The structure of this paper is as follows. A brief description of the model is offered in section 2. This is followed by an account of the model spin-up (section 3) and the method used to calculate the results (section 4). The heat budget results are then presented (section 5) and discussed (section 6), with a summary of the main results given in section 7.

2. Model

The model used is a variant of the Miami Isopycnic Coordinate Ocean Model (MICOM) described by *Bleck et al.* [1992]. Here a 2° longitude resolution has been employed encompassing 10 isopycnic layers overlaid by a Kraus-Turner [*Kraus and Turner*, 1967] type mixed layer of variable horizontal density. The thickness of all layers is a function of space and time. The model domain has 32 meridional grid points and 50 zonal grid points, covering the area between the Greenwich meridian and 100°W and 10°N and 60°N. Coastlines are straight and the bathymetry is uniform, the model ocean reaching 4000 m depth at all grid points.

The model is both thermohaline and wind driven, with the surface forcing incorporating a wind stress, a freshwater flux, a radiative heating, and a combined sensible and latent heat flux with all forcings being zonal averages. Radiative fluxes come from *Lamb and Bunker* [1982], the freshwater flux is based on *Schmitt et al.* [1989], the remaining fields being derived from the

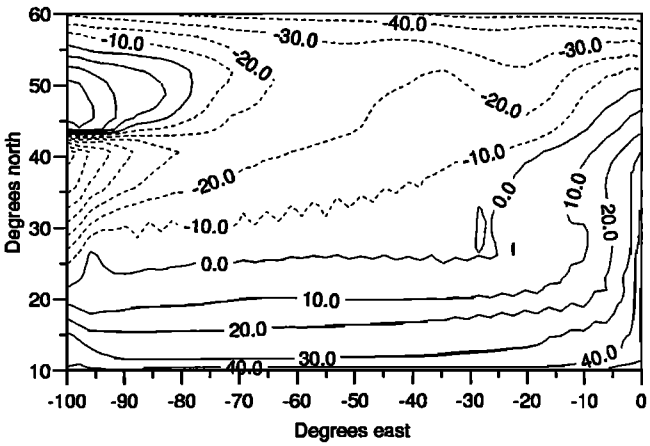

Figure 1. Total annually averaged heat content change due to surface forcing in year 33 (W/m^2).

Comprehensive Ocean-Atmosphere Data Set (COADS) [*Woodruff et al.*, 1987]. Further details are given by *Bleck et al.* [1989].

Note that though all the prescribed functions are zonally averaged, the turbulent heat flux depends upon the difference between a prescribed (pseudo) atmospheric temperature and the model mixed layer temperature and so allows zonal variation. The total surface heating is therefore a diagnostic term, the annually averaged forcing being shown in Figure 1. It should be pointed out that the formulation of the turbulent heat flux enables it to reduce the model temperature if the mixed layer is too warm and to increase the temperature if the mixed layer is too cold (as compared with the COADS data). The daily zonal wind stress may be inferred from Figure 2, which shows the Ekman transport, $-\tau_x/\rho f$ (in m^2/s).

Diffusive parameters are shown in Table 1. *Bleck et al.* [1992] argue for the inclusion of thickness diffusion in the model to represent the subgrid-scale mixing of layer thickness. This type of parameterization captures the isopycnic mixing scheme of *Gent and McWilliams* [1990] involving the advective transfer due to the slumping of isopycnals. There is no explicit diapycnic mixing in the model, although the existence of cabbeling leads to a very gradual buildup of mass in the lower layers. The potential densities (referenced to the surface) of the isopycnals are 1026.0 – 1027.8 kg/m^3 in steps of 0.2.

While the use of forcing functions derived from observed fluxes over the North Atlantic allows this modeling work to be interpreted as a study of the North Atlantic, the domain should essentially be regarded as an idealized northern hemisphere basin. The zonally averaged nature of the surface forcing, lack of a realistic coastline, 4000 m uniform depth, coarse grid resolution, and absence of inflow at the northern and southern boundaries all reduce the realism of the modeling. However, the advantages of computational efficiency, ease of use, and, most importantly, ease in understanding of the

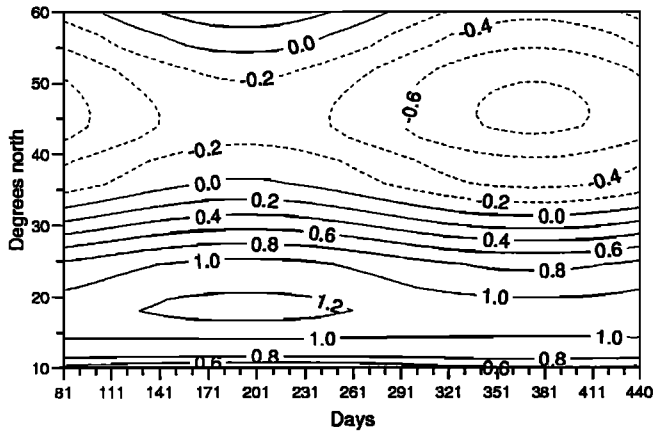

Figure 2. Daily zonally averaged meridional Ekman transport, $-\tau_x/(\rho f)$ (m^2/s). Day 81 corresponds to the vernal equinox, when the model year starts.

results are regarded as outweighing the above disadvantages.

3. Spin-Up

The model has been spun up for 34 years from a state of rest, with the heat budget study being performed in year 33. Originally, salinities were a uniform 35.0 g/kg and temperatures were such that the resulting density matched the annually and zonally averaged *Levitus* [1982] data set (as in the work by *Bleck et al.* [1992]). The model spin-up starts at the time of the vernal equinox. A graph showing the evolution of the annually and basin-averaged heat exchange with the atmosphere, calculated by averaging 12 monthly values of the heat forcing, is shown in Figure 3. From this figure it may be seen that, after an initial discharge of heat, the model has reached a state of little net surface heating by year 33. There is no guarantee that such a state would be maintained if the spin-up were extended, as the model ocean may naturally vary on a timescale of years or decades. Indeed, an analysis of the change in monthly and annual layer thickness (not shown) reveals that the isopycnic structure is still developing. Interdecadal variability in ocean models has been discussed by *Cai et al.* [1995] and *New and Bleck* [1995]. However, the feedback present in the turbulent heat flux term would tend to bring this exchange to zero. Inclusion of year 34 in Figure 3 indicates that year 33 is both in a period of little net heat forcing and little change in heat forcing and is therefore an appropriate time for a heat budget study to be carried out.

Instantaneous fields of the mixed layer velocity and temperature are shown in Figures 4a and 4b for March. As the domain is being viewed as an idealized North Atlantic, nomenclature such as the Gulf Stream, North Atlantic Current, etc., are used where appropriate. The expected double-gyre system of the North Atlantic is evident in Figure 4a, to the north of a southern buffer gyre.

As the resolution is only 2°, velocities are smaller than observed and ocean jets and currents are broader and vaguer. Nevertheless, the signature of the circulation can still be seen in the mixed layer temperature field, particularly in the isotherm distortion along the Gulf Stream and the contour congregation where the Gulf Stream and Labrador Current meet. A reasonable similarity may be seen between the above temperature field and that observed in the ocean [e.g., *Isemer and Hasse*, 1985].

Figure 5 displays a cross section of the layer thicknesses. As this particular section is in March, a number of the interior layers have been absorbed by the mixed layer. Although the details of such sections would vary spatially and seasonally, the bottom two layers of the model consistently occupy the bulk of the model depth. These will therefore be viewed as representing the deep and abyssal ocean, with layers 2–9 forming the model thermocline.

The March mixed layer depth is shown in Figure 6. It can be seen that there are no areas where the mixed layer exceeds 900 m. Examination of relevant winter cross sections (not shown except for the west-east section at 30°N in Figure 5) suggests that convection does not penetrate through the thermocline anywhere in the model. This is in part due to the model domain only

Table 1. Diffusive Parameterization

Parameter	Value, cm/s	Diffusivity, m^2/s
Thickness diffusion velocity	0.5	1000
Momentum dissipation velocity	2.0	4000
Temperature and salinity mixing velocity	1.0	2000
Deformation dependent viscosity	2.0	N/A

Diffusive parameters are described by velocities. Equivalent diffusivities may be calculated by multiplying these diffusive velocities by the grid scale, taken here to be 2×10^5 m. The deformation-dependent viscosity is also dependent on the horizontal velocity gradients, so no typical diffusivity is given for this parameter. It is only used when the diffusivity becomes larger than the background diffusion, given by the momentum dissipation velocity.

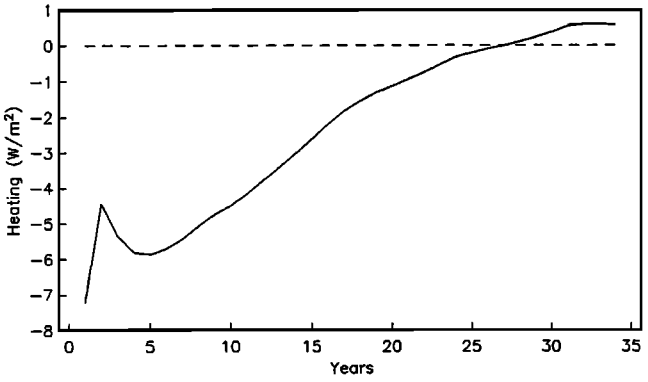

Figure 3. Annual- and basin-averaged surface heating in the model.

reaching 60°N and in part because the 2° resolution is not sufficient to resolve the localized nature of deep convection but would tend instead to smear out extreme climatic events.

The maximum heat transport in the model is 0.4 PW at 25°N. There is, though, no heat transport at the southern boundary of 10°N where observational estimates suggest a heat transport of perhaps 1.0 PW [*Isemer et al.*, 1989], admittedly with an uncertainty of at least 0.5 PW. Similarly, there is no heat transport at the northern boundary at 60°N where observational estimates are approximately 0.2 PW [*Isemer et al.*, 1989]. Given these boundary conditions, the model heat transport compares reasonably with the estimate of 1.2±0.3 PW at 24°N from *Hall and Bryden* [1982]. *Wang et al.* [1995] suggested, from experiments with a barotropic model, that decreasing resolution may restrict heat transport. However, *Cox* [1985] showed that decreasing horizontal resolution in a multilevel model only changed the nature of the heat transport, not its magnitude. Certainly, the model of *Sarmiento* [1986] achieved a greater heat transport than this model (0.86 PW at 24°N), despite having the same resolution, as it incorporated a larger domain (30°S – 68°N) and therefore greater heat transport at 10°N. *New et al.* [1995] obtained a slightly smaller maximum heat transport (~ 0.67 PW) than *Sarmiento* [1986] in a similarly sized domain (20°S – 80°N) with an isopycnic model, despite having a higher resolution of approximately 0.5° – 1°. It therefore seems likely that, though the heat transport may be restricted in this model by the coarse resolution, the restriction is probably not a significant one.

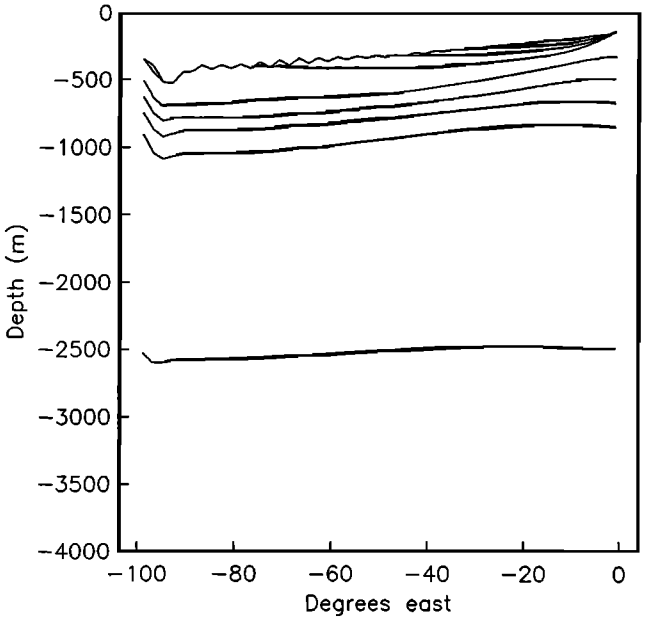

Figure 5. Eastward section of layer thickness across 30°N in March, year 33. Note that the ocean floor is at 4000 m.

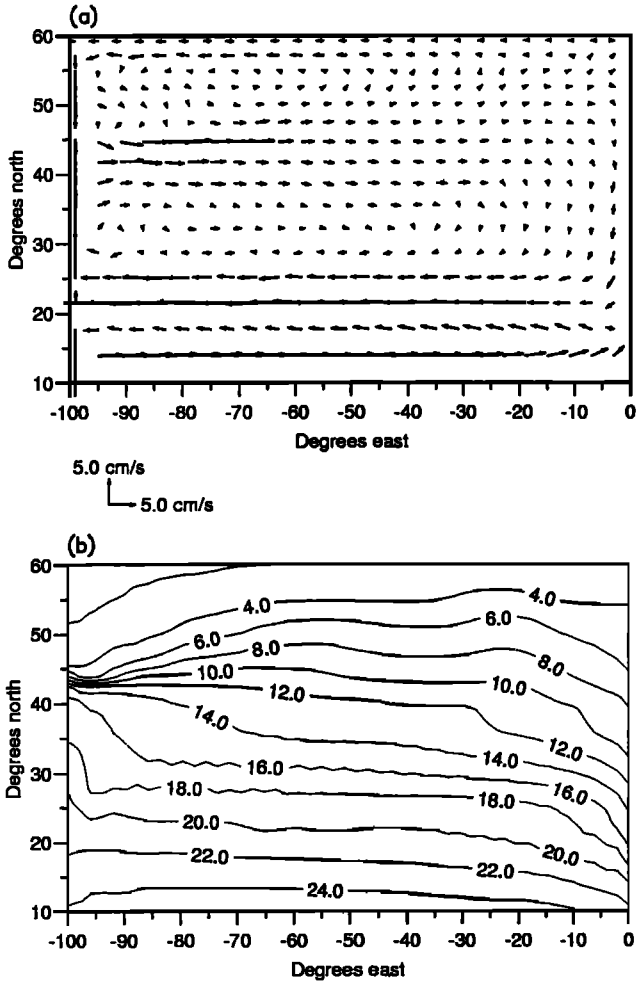

Figure 4. (a) Velocity of the mixed layer in March, year 33. Only every other grid point is plotted. A zonal 1-2-1 filter has been applied to the velocities. (b) Temperature of the mixed layer in March, year 33 (degrees Celsius).

4. Calculation of Results

The results of the heat budget analysis have been calculated in two separate ways. All heat content changes, except for the explicit effects of the Ekman flow, have been calculated on-line. That is, at each part of the model where a heat content change occurs, the heat

content of the entire water column has been calculated both before and after the change, the difference indicating the magnitude of the heat content change. This method has the distinct advantage of giving highly accurate results and enabling the heat budget to be broken down into as many constituent parts as desirable. Those to be presented herein are the total advective heat content change, the diffusive change, and the total change due to surface heating. Of these, the surface forcing is made up of both the radiative and the turbulent heat fluxes, described in section 3.

The advective contribution to the heat budget may also be split into the constituent parts of Ekman advection, caused by wind stress effects, and other advection, defined as the residual of the total advective effects less the Ekman advective effects. This non-Ekman advection is obviously similar to the geostrophic advection but is not identical, as it includes, for example, time dependence. Thickness diffusion, which may change the heat content of a water column by increasing or decreasing the thickness of a layer of a particular temperature, is included in the advection results. The Ekman advection, in contrast to the other results, is initially calculated diagnostically using the model-produced temperature field. In order to be explicit about the assumptions used to perform this diagnostic calculation of Ekman advective change, incorporating both (horizontal) Ekman transport and (vertical) Ekman pumping, a derivation of the Ekman heat content change equation is given below. Note that the calculation is performed in (x, y, z) coordinates.

From the starting point of the adiabatic equation for temperature conservation, the continuity equation, and the equation for heat content change, an equation for the advective heat content change of a water column may be written as

$$\frac{\partial H_c}{\partial t} = -\rho C_p \left[\int_{-h_e}^{0} \frac{\partial (u_e T)}{\partial x} + \frac{\partial (v_e T)}{\partial y} + \frac{\partial (w_e T)}{\partial z}\, dz + \int_{-D}^{-h_e} \frac{\partial (u_e T)}{\partial x} + \frac{\partial (v_e T)}{\partial y} + \frac{\partial (w_e T)}{\partial z}\, dz + \int_{-D}^{0} \frac{\partial (u_r T)}{\partial x} + \frac{\partial (v_r T)}{\partial y} + \frac{\partial (w_r T)}{\partial z}\, dz \right], \quad (1)$$

where H_c is the heat content of a water column; t is time; ρ is density, assumed to be constant; C_p is the specific heat capacity of water, also assumed to be constant; T is temperature; and $z = 0$ is the sea surface, $z = -h_e$ is the base of the Ekman layer, and $z = -D$ is the seafloor, all of which are assumed to be invariant in space and time. The velocity vector $\mathbf{u} = (u, v, w)$ is split up into a (three-dimensional) Ekman part $\mathbf{u}_e = (u_e, v_e, w_e)$ and a residual velocity $\mathbf{u}_r = (u_r, v_r, w_r)$, representing all the other velocity constituents (principally, but not exclusively geostrophic), defined as

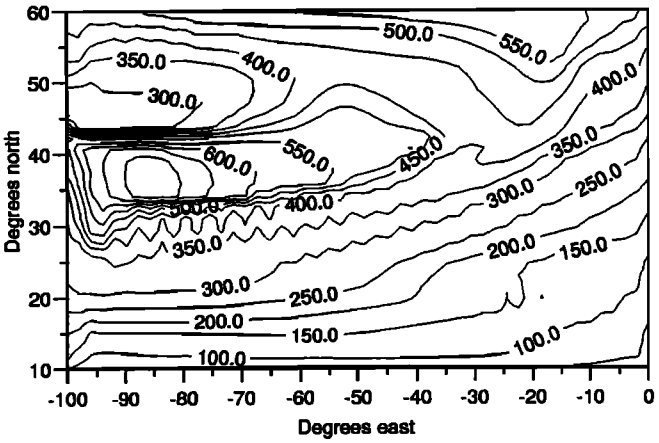

Figure 6. Mixed layer depth in March, year 33 (meters).

$\mathbf{u}_r = \mathbf{u} - \mathbf{u}_e$. For convenience this residual velocity $\mathbf{u}_r$ is termed the non-Ekman velocity.

The meridional Ekman mass transport M_y is linked to the wind stress through the expression

$$M_y = \rho \int_{-h_e}^{0} v\, dz = -\frac{\tau_x}{f}, \quad (2)$$

where τ_x is the zonal wind stress and f is the Coriolis parameter.

When there is no meridional wind stress and both Ekman and non-Ekman vertical velocities at the sea surface and the seafloor are assumed to be zero, there are no explicit horizontal Ekman velocities below the Ekman layer, and the Ekman layer is assumed to be always contained within the mixed layer, (1) and (2) may be combined to give

$$\frac{\partial H_c}{\partial t} = -\rho C_p \left(-T_e \frac{1}{\rho} \frac{\partial (\tau_x / f)}{\partial y} - \frac{\tau_x}{f\rho} \frac{\partial T_e}{\partial y} + \int_{-D}^{0} T \frac{\partial u_r}{\partial x} + T \frac{\partial v_r}{\partial y}\, dz + \int_{-D}^{0} u_r \frac{\partial T}{\partial x} + v_r \frac{\partial T}{\partial y}\, dz \right), \quad (3)$$

where T_e is the temperature of the Ekman layer. Noting that the (three-dimensional) Ekman flow within the Ekman layer will be nondivergent, as will be the total flow in the water column, gives

$$-w_e|_{z=-h_e} = \frac{1}{\rho} \frac{\partial (\tau_x / f)}{\partial y} = \int_{-D}^{0} \frac{\partial u_r}{\partial x} + \frac{\partial v_r}{\partial y}\, dz. \quad (4)$$

Thus the vertical Ekman velocity at the base of the Ekman layer, $-w_e|_{z=-h_e}$, induced by a wind-driven convergence of fluid in the Ekman layer must be balanced by a compensatory flow, equal to the Ekman pumping, somewhere in the water column. Although this compensatory flow is not here defined as an explicit component of the Ekman flow, it is an indirect consequence of water being forced to leave the water column as a result

of a convergence in the Ekman layer of a finitely deep ocean.

Equation (3) may be further simplified by exploiting the concept of a reference temperature indicative of the water that is leaving the water column at depth in response to the convergence of water in the Ekman layer and the consequent Ekman pumping. As the mass flow is known from (4), then assuming that the entire compensatory, divergent flow is equally distributed throughout a particular depth range and denoting the average temperature of this water as T_{ref} allows (3) to be reduced to

$$\frac{\partial H_c}{\partial t} = C_p \frac{\tau_x}{f} \frac{\partial T_{\text{ml}}}{\partial y} + C_p (T_{\text{ml}} - T_{\text{ref}}) \frac{\partial (\tau_x / f)}{\partial y} - \rho C_p \int_{-D}^{0} u_r \frac{\partial T}{\partial x} + v_r \frac{\partial T}{\partial y} dz, \quad (5)$$

where T_{ml} is the temperature of the mixed layer of the water column. Note that this assumption precludes the possibility of other divergences and convergences in the water column that might exist independently of any Ekman-induced activity that is taking place. The right-hand side of (5) therefore ignores any heat content changes that would occur owing to non-Ekman flow entering the column at one depth with an equal quantity of water leaving the column at another (colder) depth, though such an effect may be expected to be small. Thus the first term on the right-hand side represents the effects of Ekman transport and is confined to the Ekman layer. The second term represents the effects of Ekman pumping of warm surface waters into the cooler thermocline and abyssal waters and is in part determined by the assumed temperature, T_{ref}, at which the compensatory flow leaves the water column. Advective effects of all other types of (nondivergent) flow in the water column are represented by the third term.

This is the diagnostic equation from which the Ekman contribution to the heat budget may be calculated. Such a calculation may, in principle, be made from either model or real data [e.g., *Marshall et al.*, 1993] as long as the fields of wind stress and temperature are known. As the total heat content change of a water column is calculated on-line, along with the diffusive and source terms, the non-Ekman advective term may be inferred by a simple subtraction. For the heat budget results presented herein the assumption is made that there is little seasonal change in the temperature of the deep ocean [cf. *Bryden et al.*, 1991] and thus that the compensatory flow takes place wholly in the thermocline, i.e., layers 2–9 of the model, and T_{ref} is calculated by taking a layer-thickness-weighted average of the temperature of the thermocline waters. The question of what is the appropriate reference temperature is addressed in more detail in section 6.2.

The heat budget calculations carried out within the model have been performed at every time step and averaged over 30-day periods to give 12 monthly values. From these, annual averages can be calculated. Ekman results have been calculated from similarly averaged mixed layer temperatures, although the reference temperatures for each month have been calculated from only two values per month. However, as the seasonable variation in the thermocline temperature field is both smooth and small, this approximation is not expected to compromise the accuracy of the results to any significant degree. Monthly zonal averages were also obtained and are shown subsequently.

5. Results

5.1. Annual Averages

Figures 1, 7a, and 7b show the annually averaged heat content change caused by surface heating, total advection, and temperature diffusion, respectively. Values, particularly those over ocean jets, are smaller than observed values would be owing to the resolution used, hence the figures should be viewed in a comparative rather than an absolute sense. Figure 1 (surface heating) includes both turbulent (model dependent) and radiative (model independent) heating, the latter gener-

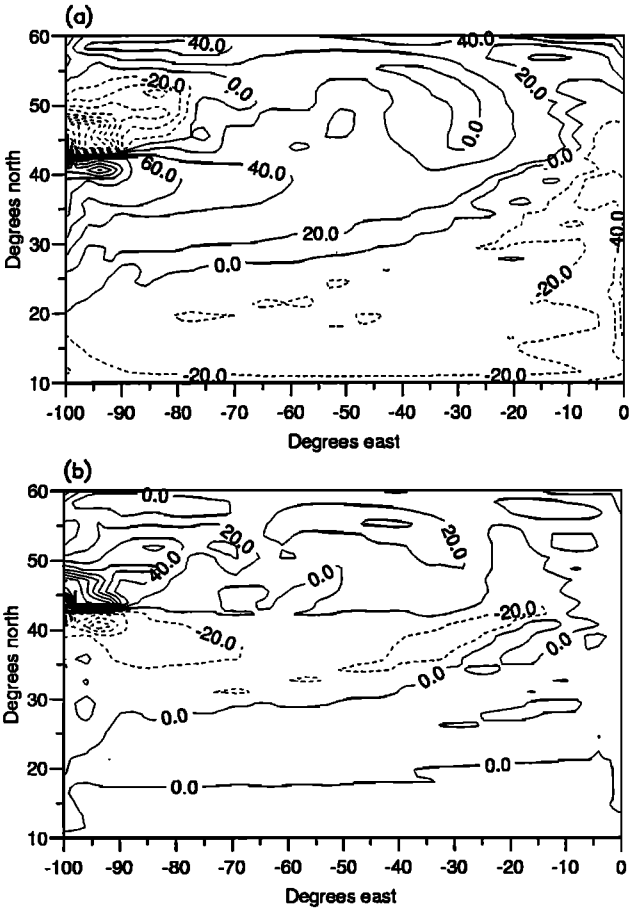

Figure 7. Total annually averaged heat content change due to (a) total advection (including thickness diffusion) and (b) temperature diffusion (W/m^2). A zonal 1-2-1 filter has been applied to both fields.

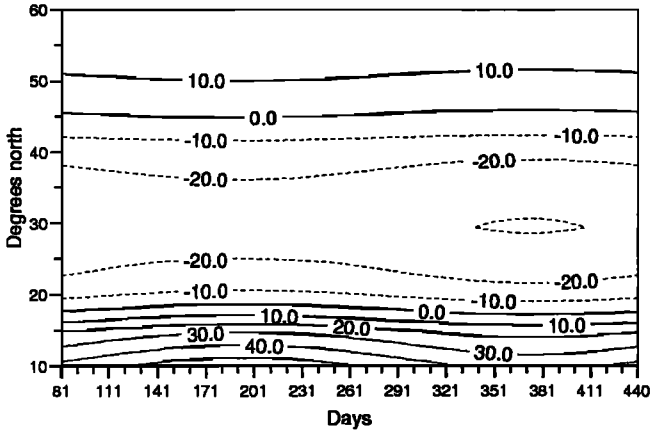

Figure 8. Daily Ekman pumping (positive upward), $-1/\rho\ \partial(\tau_x/f)/\partial y$ (m/yr). Day 81 corresponds to the vernal equinox, when the model year starts.

ally being a source of heat, while the former is more usually a heat sink. Deviations from a zonal average are induced by the pattern of mixed layer temperature in which asymmetries are produced by the velocity field. Hence superimposed on the picture of southerly warming and northerly cooling is increased cooling along the Gulf Stream and North Atlantic Current and warming in the vicinity of the Labrador Current and the cold eastern boundary current of the subtropical gyre.

The influence of the ocean currents is shown more clearly in Figure 7a, which depicts the advective effect on the heat budget. There is a large degree of heating in the Gulf Stream with heat being brought farther north along the path of the North Atlantic Current. In the northwest corner, where the Labrador Current brings cold water southward, a significant cooling can be seen. This plot is broken into its Ekman and residual parts.

The diffusive heat content change (Figure 7b) roughly follows the gyre structure, with cooling present in the subtropical gyre and warming in the subpolar gyre. Both cooling and warming intensify near the Gulf Stream separation, where the temperature gradient changes rapidly. Although there are some discrepancies in the details, particularly in the southern buffer gyre, the diffusion, on average, fluxes heat from the south to the north of the domain.

The seasonal, zonally averaged cycle of meridional Ekman transport, $-\tau_x/\rho f$, is shown in Figure 2. It can be seen from (5) that the product of (the negative of) this term, the meridional temperature gradient, the specific heat, and the density ($C_p \times \rho \sim 4 \times 10^6$) gives the heat content change due to Ekman transport. Figure 8 is similar but represents the Ekman pumping, $-1/\rho\ \partial(\tau_x/f)/\partial y$ (in m/yr). Equation (5) reveals that (the negative of) this term multiplied by the temperature difference between the water in the Ekman layer and the water in the Ekman compensatory flow and the product of specific heat capacity and density is the heat content change caused by Ekman pumping. The Ekman pumping values are rather on the low side compared with those from the *Isemer and Hasse* [1985] climatology and those given by *New et al.* [1995] using the *Hellermann and Rosenstein* [1983] wind fields.

The annually averaged effects of Ekman transport and Ekman pumping calculated using these fields are shown in Figures 9a and 9b. As mentioned above, in Figure 9b it has been assumed that the Ekman compensatory flow is wholly in the thermocline. Northward Ekman flow in regions of easterlies should heat up the water column by bringing with it warmer southern water. Similarly, westerlies should be accompanied by a heat loss. This pattern can be seen in Figure 9a, with the heating and cooling regions being separated by zero lines corresponding to lines of zero wind stress shown in Figure 2. The increase in cooling at about 43°N in Figure 9a is caused by the presence of the North Atlantic Current. Here the isotherms are more tightly packed, so the (nearly perpendicular) Ekman flow is more effective at reducing the heat content.

In regions of convergent Ekman flow there will be Ekman pumping and a consequent transferal of warmer surface waters to the deeper ocean at the expense of cooler submixed layer water, causing a net heat content rise in the water column. Divergent Ekman flow and

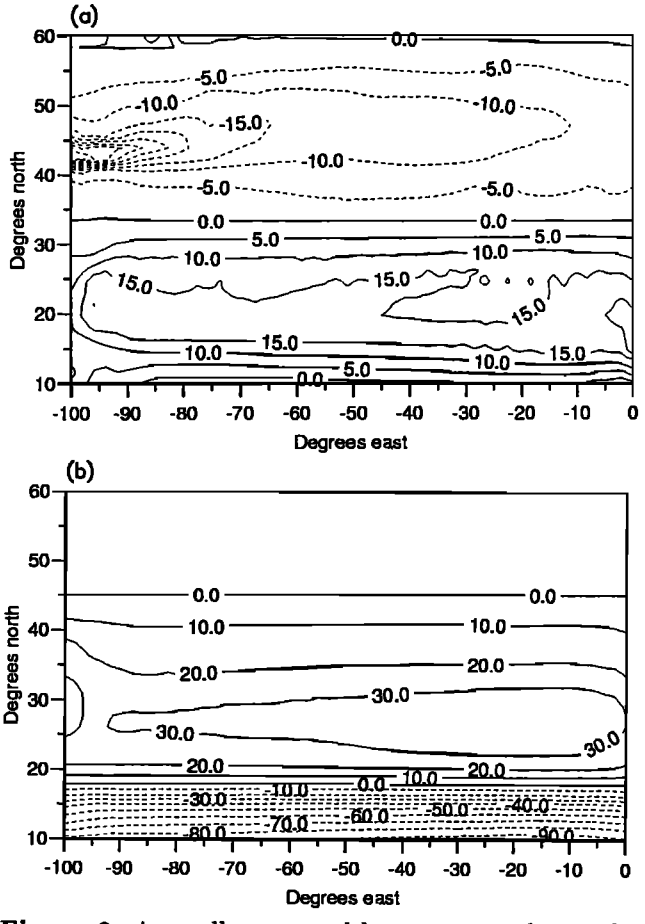

Figure 9. Annually averaged heat content change due to (a) Ekman transport and (b) Ekman pumping, assuming compensatory flow in the thermocline (W/m^2).

Ekman suction would induce a cooling, at least in areas where the surface water is warmer than the lower waters. This may not be true in some northerly regions in winter where extreme surface cooling may cause the opposite to occur, water column stability being maintained by saltier water existing in the interior. In Figure 9b, considerable heating can be seen throughout the subtropical gyre where the Ekman flow converges. Although the vertical velocity is small, amounting to, say, 30 m/yr (Figure 8), the crucial aspect is the steep vertical temperature gradient allowing only a small transfer of water to have a noticeable effect on the heat budget. There is also strong cooling to the south, although the effects in the subpolar gyre are relatively small. The bias to larger effects in the southern half of the domain is in part caused by the change in $1/f$ in these latitudes and in part reflects the increased stratification of the warmer southern waters. The zero lines correspond to those in Figure 8 where there is no meridional gradient of zonal wind stress. As the actual Ekman pumping (Figure 8) is somewhat less than that used elsewhere [e.g., *Isemer and Hasse,* 1985], it seems likely that the heat content change caused by the Ekman pumping should also be greater than that shown here.

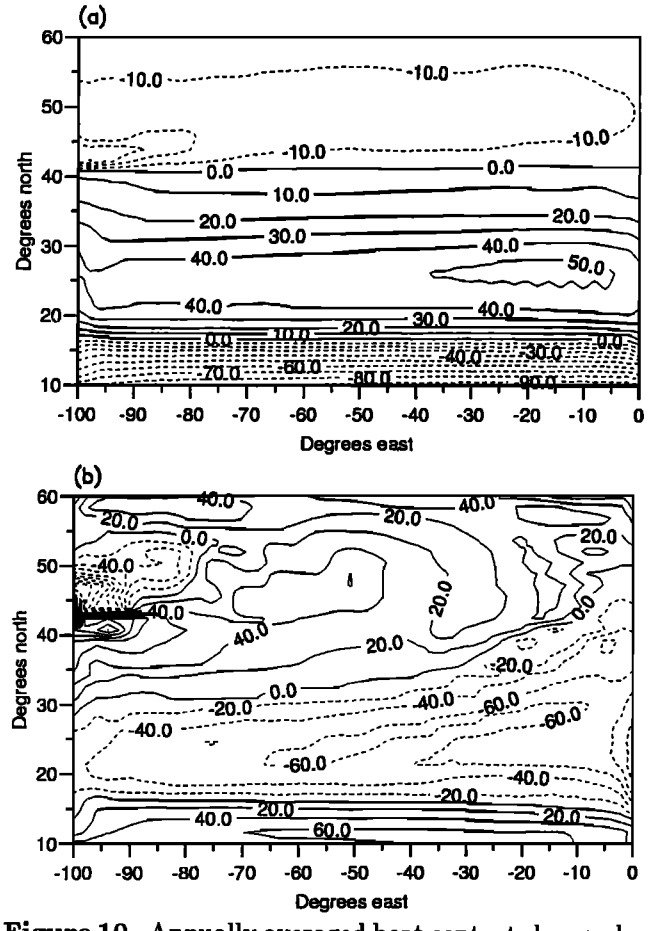

Figure 10. Annually averaged heat content change due to (a) combined Ekman transport plus Ekman pumping and (b) non-Ekman advection, when assuming the Ekman compensatory flow is in the thermocline (W/m^2).

Summing these Ekman effects leads to Figure 10a. Throughout much of the subtropical and subpolar gyres the two different facets of the Ekman flow have the same effect on the heat budget. However, in the northern part of the subtropical gyre the heating due to convergent Ekman flow pumping warmer waters into the thermocline is modified by the simultaneous (horizontal) transport of cooler water into the Ekman layer. These results may be subtracted from the overall advective heat content change (Figure 7a) to indicate the heat content change due to non-Ekman (principally geostrophic) advection. In general, geostrophic advection is expected to bring heat to the Gulf Stream and along the North Atlantic Current and take heat away in the Labrador Current. There should also be a small heat loss in the interior of the subtropical gyre and a small heat gain in the subpolar gyre, where slight southerly and northerly flows may be expected to exist, respectively, in volume balance with the western boundary currents. This non-Ekman advection is shown in Figure 10b, and this general pattern can be seen, although the rather broad North Atlantic Current leads to warming in a good proportion of the northern subtropical gyre. It is noted that magnitudes are comparable to those in the Ekman results, although the more vigorous heat content changes are often in different parts of the domain.

5.2. Spatial Averages

As can be seen from a comparison of Figures 1, 7b, 9a, 9b, and 10b, different regions of the model North Atlantic are controlled by different heat balances. This result is more clearly demonstrated in Figure 11, which summarizes the heat content changes caused by diffusion (D), Ekman pumping (EP), Ekman transport (ET), non-Ekman advection (NA), and surface heating (S). In this figure the domain has been divided into 20 mutually exclusive boxes, each of 10 zonal by 8 meridional grid boxes, in which the above results were spatially averaged, the average heat change caused by each process being indicated at each box. Font size represents the magnitude of the change, with small lettering suggesting a change of 10–15 W/m^2, medium lettering indicating 15–25 W/m^2, large lettering denoting 25–35 W/m^2, and very large lettering suggesting changes of more than 35 W/m^2. The largest positive change is written to the north of each box; the largest negative change is to the south. Any changes of less than 10 W/m^2 are not shown.

Along the North Atlantic Current and in the subpolar gyre the expected balance between geostrophic advection, bringing heat into the region and surface fluxes that extract the heat from the region, is evident. Ekman transport is responsible for a loss of heat where it takes colder water across the polar front. There is also a little diffusive warming in these regions, as the model numerics tend to diffuse heat from the warm south to the cold north.

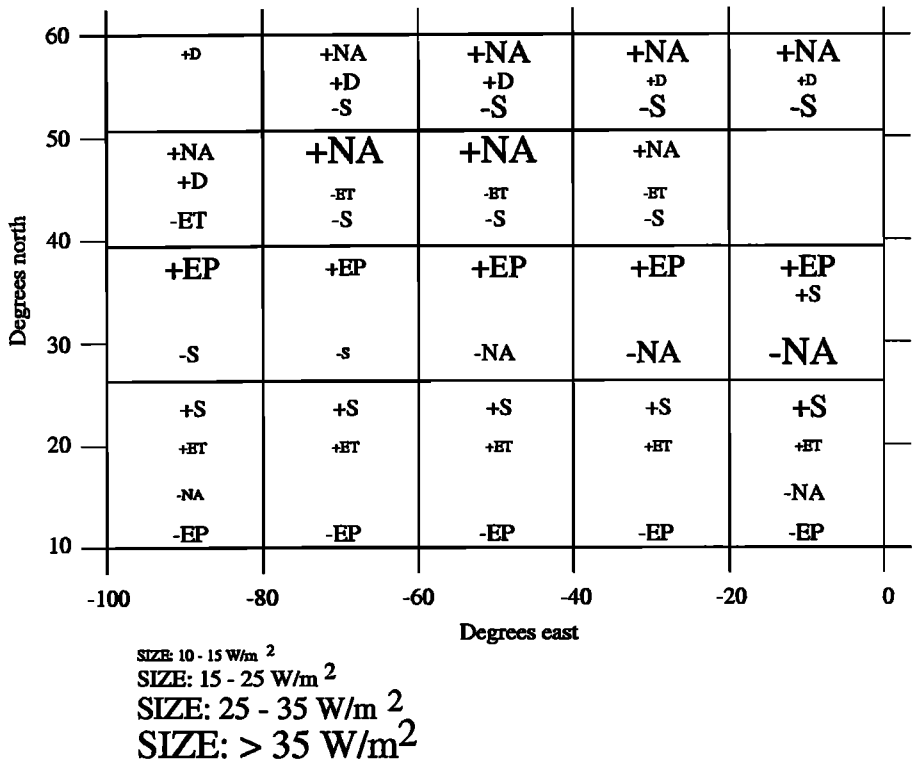

Figure 11. Summary of the spatially and annually averaged heat budget in year 33. The boxes shown represent the boxes in which the spatial averaging has been carried out. The font size indicates the amount of heat content change that has taken place. Changes of less than 10 W/m^2 are not shown. The processes represented are temperature diffusion (D), Ekman pumping (EP), Ekman transport (ET), non-Ekman advection (NA), and surface forcing (S).

However, quite different behavior is demonstrated in the subtropical gyre, where the net surface heating is small. There, Ekman pumping, which was negligible farther north, is the largest heat source throughout the region. This heat input is principally balanced by non-Ekman advection, except near the Gulf Stream, where heat is lost through the ocean surface. In the south of the domain, Ekman pumping is again dominant, but here it acts as a heat sink, while both surface heating and, to a lesser extent, Ekman transport, are responsible for heat being brought into the region. However, as $1/f$ becomes infinite toward the equator, the formulation breaks down there, so results in the south need to be treated with some caution. As noted above, the rather weak wind stress fields may be causing an underestimate in the degree of warming caused by Ekman pumping.

5.3. Zonal Averages

Attention may now be turned to the seasonal cycle. Zonally averaged results for each month (30 days) are shown in Figures 12a–12e. These represent surface heating, diffusion, Ekman transport, Ekman pumping, and non-Ekman advection, respectively. Month "3.2" represents the 30 days from March 21. The Ekman and non-Ekman parts have been obtained using the same method as for the annual results.

It is immediately striking that the character of the surface heating (Figure 12a) is quite different from the other results. This displays an obvious seasonal cycle and a heating and cooling nearly an order of magnitude larger than any of the other effects. There is a larger meridional variation in the winter than in the summer. The diffusion (Figure 12b) does not exhibit an obvious seasonal cycle, but a diffusive transfer of heat from the subtropical gyre to the subpolar gyre can be seen. South of 35°N, the net diffusive effects are small.

Both Ekman terms display a muted seasonal cycle. They also exhibit a strong latitudinal dependence. The magnitude of the Ekman transport (Figure 12c) is seen to follow the changes in wind stress strength (Figure 2). However, it is noticeable that the maximum heating and cooling due to Ekman pumping (Figure 12d) occur during the late summer, despite this not being when the meridional gradient in the wind stress is at its steepest (Figure 8). It may therefore be inferred that the seasonal cycle is more affected by the degree of thermocline stratification than by the change in wind stress. A similar result was obtained by *Paillet and Arhan* [1996] for a region off the western coast of Iberia. In winter it is interesting to note that Ekman suction produces

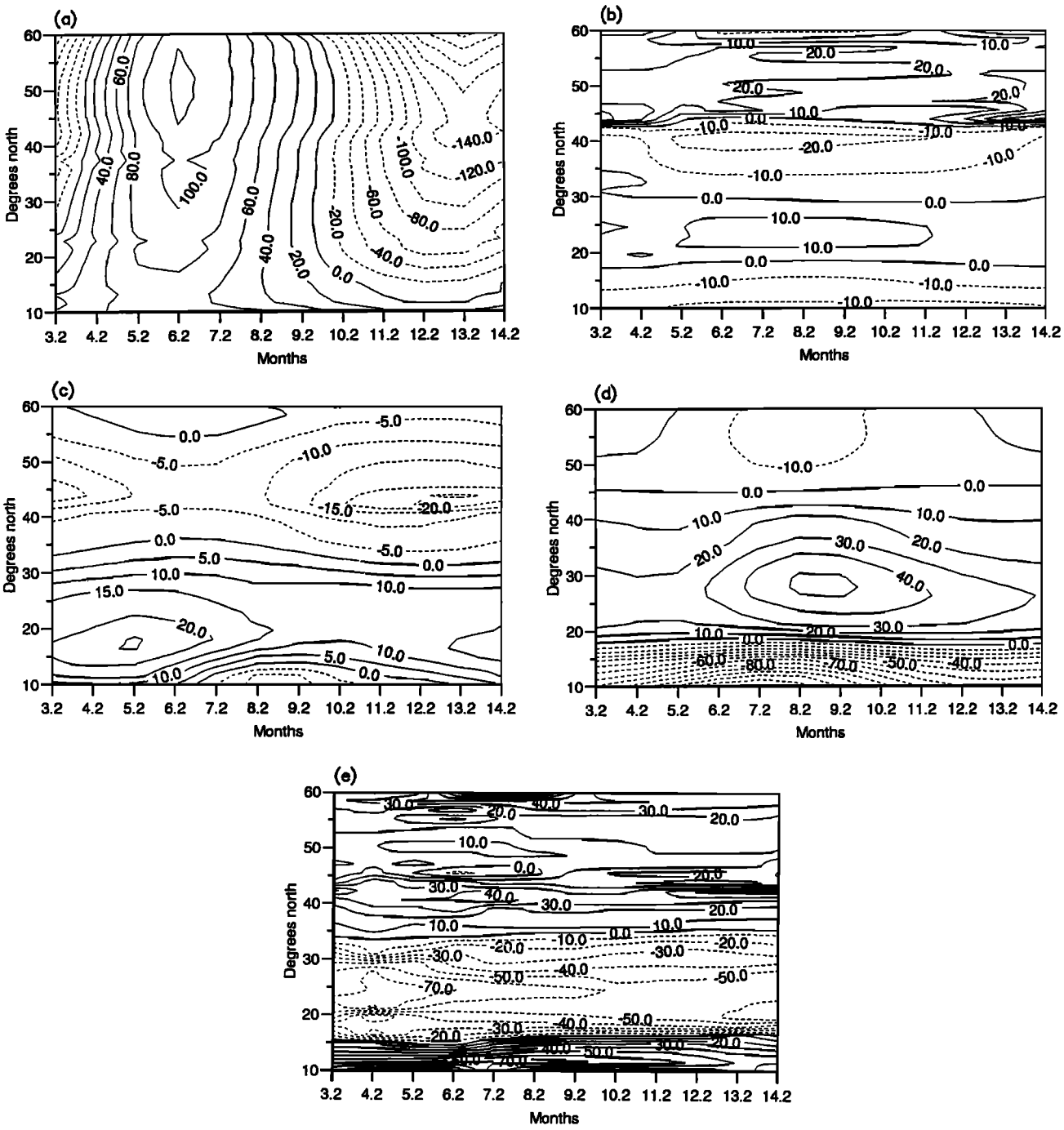

Figure 12. Zonally averaged monthly heat content change due to (a) surface heating, (b) temperature diffusion, (c) Ekman transport, (d) Ekman pumping, and (e) non-Ekman advection (W/m^2). Data represent monthly averages, thus month "3.2" denotes the average of the 30 days between March 21 and April 20 (the first month of the model run). The midpoint of this month corresponds to day 96 of the conventional year.

a slight warming in the north of the subpolar gyre as a result of the surface layer there being slightly colder than the deeper ocean. There is little seasonal cycle in the non-Ekman advection (Figure 12e), but, discounting the very south of the domain, it may be seen that the effect of this type of advection is to transport heat from the south to the north.

5.4. Subduction Rates

Although there is no deep convection produced in the experiment, there is widespread subduction. Following *Marshall et al.* [1993], the annual subduction rate S_{ann} may be defined as

$$S_{\text{ann}} = -\overline{w_{\text{ek}}} + \frac{\beta}{f}\int_{-H}^{0} \overline{v}\, dz - \overline{\mathbf{u}_H}\cdot\nabla H, \qquad (6)$$

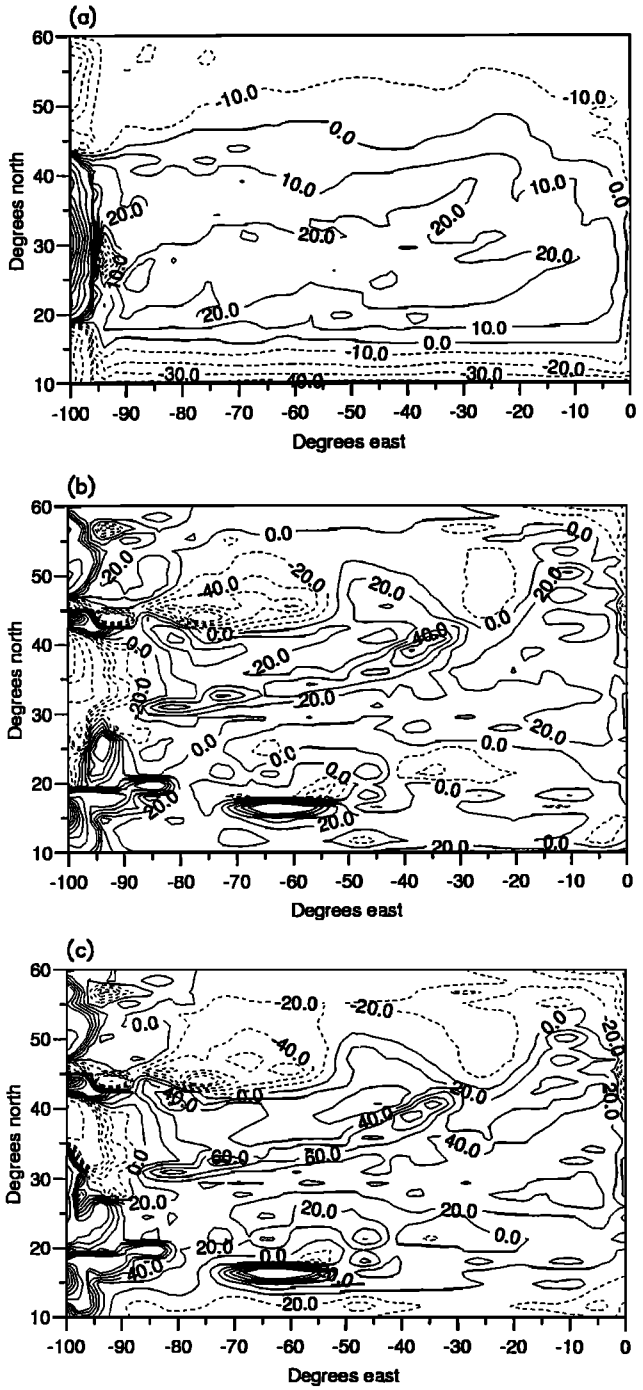

Figure 13. Annual subduction rates, (a) $-\overline{w_H}$, (b) $-\overline{u_H}\cdot\nabla H$, and (c) S_{ann} (m/yr). Contours are 10 to ±100 m/yr and then every 50 m/yr in Figure 13a and 20 to ±100 m/yr and then every 100 m/yr in Figures 13b and 13c.

where w_{ek} is the Ekman pumping, β is the gradient of the Coriolis force, and H is the maximum mixed layer depth, taken here to be the depth at the end of the first month (i.e., April 20). Overbars denote annual averages. The first two terms on the right-hand side combine to give $-w_H$, the vertical velocity at the base of the mixed layer in winter. The final term on the right-hand side represents the lateral advection of fluid through the sloping base of the hibernal mixed layer.

Values for $-\overline{w_H}$, $-\overline{u_H}\cdot\nabla H$, and S_{ann} are shown in Figures 13a–13c. Daily Ekman pumping values are shown in Figure 8. Similar pictures are shown by both *Marshall et al.* [1993] and *New et al.* [1995]. The pattern of vertical velocity follows the gyre structure, with downward motion being constrained to the subtropical gyre and upward motion elsewhere. A vertical velocity of 10–20 m/yr is present throughout most of the subtropical gyre. This is relatively small compared with both *Marshall et al.* [1993] and *New et al.* [1995], reflecting the low values of Ekman pumping shown in Figure 8. The effects of lateral subduction are shown in Figure 13b. Most of the subtropical gyre is subject to a lateral subduction of a few tens of meters, with lenses of increased subduction evident where the maximum mixed layer depth shoals rapidly in the northern part of the gyre (see Figure 6). Negative subduction takes place within the Gulf Stream and North Atlantic Current. Combining the vertical and lateral subduction terms gives the total annual subduction rate shown in Figure 13c. The pattern is similar to that for lateral subduction alone, although the values are enhanced by the vertical velocity terms. Qualitatively, these figures compare well with those of *Marshall et al.* [1993] and *New et al.* [1995], although the values tend to be smaller. The similarity with the *New et al.* [1995] result is particularly encouraging, given their use of higher resolution and a more realistic domain and bathymetry.

6. Discussion

6.1. Annual Averages

In the subtropical gyre there is subduction through Ekman pumping and lateral transfer through the mixed layer [*Marshall et al.*, 1993]. The subduction requires a supply of buoyancy to the mixed layer. However, as the surface heating is small across the subtropical gyre, it has been argued that the principal supply of heat to the mixed layer enabling this subduction to take place comes through the Ekman transfer [*Marshall et al.*, 1993; *Marshall and Marshall*, 1995]. The results in this paper support their argument, demonstrating the importance of Ekman pumping, in particular, to the subduction process in the North Atlantic subtropical gyre.

Furthermore, *Paillet and Arhan* [1996] proposed that the bulk of the North Atlantic mode water formation occurs in the region where the net buoyancy given to a fluid column above the base of the winter mixed layer changes from negative to positive. This net buoyancy may come from either the surface fluxes or through Ekman transfer. Thus, as fluid crosses this "line of net zero buoyancy flux to the mixed layer," there is a large reduction in the maximum winter mixed layer depth. This line of net zero buoyancy flux to the mixed layer

in the North Atlantic was calculated by *Marshall et al.* [1993, Figure 14] and can be seen to snake diagonally across the subtropical gyre. As the line of net zero heating of the mixed layer acts as a tight constraint on this line of net zero buoyancy flux to the mixed layer, which also includes the effects of freshwater fluxes, it may therefore be understood that any alterations in the effects of Ekman pumping will change the location of this line and hence the temperature and salinity of the water subducted into the thermocline.

It should be noted that in the work of *Marshall et al.* [1993] and *Paillet and Arhan* [1996] the reference temperature used to deduce the effects of Ekman pumping was that of the March mixed layer, as both groups of authors were concerned with the effects on subduction. In this contribution, where the emphasis is on the heat budget, the slightly colder reference temperature of the thermocline has been used, resulting in slightly larger heat content changes. The question may therefore be asked about what is the appropriate reference temperature for Ekman pumping, or more precisely, at what depth does water diverge (converge) in the water column in response to Ekman convergence (divergence) at the surface. This depth need not be the same everywhere.

6.2. Ekman Compensatory Flow

In order to test the sensitivity of the heat content change caused by Ekman pumping to the depth of the compensatory flow, two alternative assumptions on the depth of the compensatory flow have been made. The first is that the compensatory divergence takes place throughout the entire water column beneath the mixed layer. Such an assumption allows a recalculation of the effects of Ekman pumping on the heat budget, resulting in Figure 14a. From this figure it may be seen that the magnitude of heat content change is magnified (compared with Figure 9b), as would be expected from using a lower average reference temperature. Thus the effect of Ekman pumping could plausibly be greater than that suggested above. Correspondingly, a change to a divergence only in the upper thermocline would result in a lessening of the effect. In order to indicate the full range of the effects of Ekman pumping, the calculation has been made using the reference temperature to be that of model layer 2. The results are shown in Figure 14b. Note, though, that this is unrealistic in the present model configuration as layer 2 does not always exist, as it may be engulfed by the mixed layer for certain periods of the year. Despite this, its theoretical temperature is always known.

The study by *Böning and Herrmann* [1994] suggests the possibility that the mean response of the water column, being dictated by baroclinic timescales, is within the thermocline, whereas seasonally, the water column responds barotropically to changes in the wind stress, resulting in a depth-averaged compensatory flow. However, as the annual mean is significantly larger than the seasonal change in wind stress used in this model (Figure 2), calculating the heat content change by using an annual mean of the Ekman pumping with a thermocline reference temperature and a seasonal deviation from the mean with a depth-averaged reference temperature (not shown) causes only a slight difference from using a thermocline reference temperature with the entire Ekman pumping.

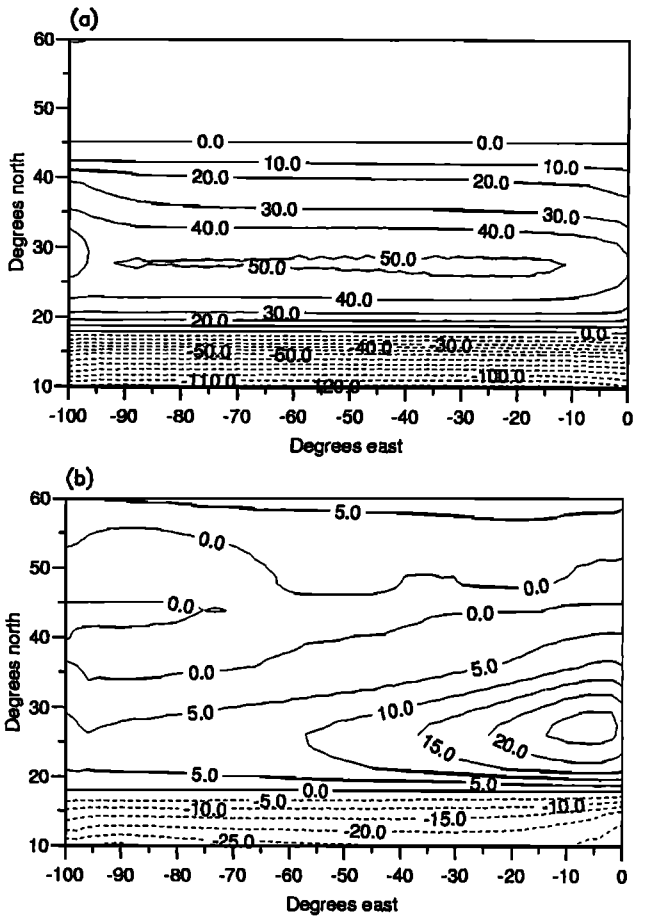

Figure 14. Annually averaged heat content change due to Ekman pumping, assuming (a) a compensatory flow at all depths and (b) a compensatory flow in layer 2 (W/m^2).

An on-line estimate of the Ekman effects and the depth of the compensatory flow may also be attempted. The continuity and temperature conservation equations may be written for a water column of N layers as

$$\sum_{k=1}^{N} \frac{\partial \Delta p_k}{\partial t} + \sum_{k=1}^{N} \nabla_s \cdot (v_k \Delta p_k) = 0, \quad (7)$$

$$\sum_{k=1}^{N} \frac{\partial (T_k \Delta p_k)}{\partial t} + \sum_{k=1}^{N} \nabla_s \cdot (v_k T_k \Delta p_k) = 0, \quad (8)$$

where $v_k = (u_k, v_k)$ is the (two-dimensional) horizontal velocity vector (measured in the projection onto a horizontal plane) of layer k, T_k is the temperature of the

layer, Δp_k is the pressure thickness of the layer, and s is a generalized vertical coordinate with subscript s indicating that this is held constant during the partial differentiation. Equation (8) ignores diffusive and source terms and thus represents only the advective effect on the temperature. See *Bleck et al.* [1992] for a derivation of these equations for an individual layer.

By splitting the velocity of the mixed layer into an Ekman part $\boldsymbol{v}_e$ and a part due to other forces $\boldsymbol{v}_r$, such that $\boldsymbol{v}_1 = \boldsymbol{v}_e + \boldsymbol{v}_r$, assuming the sum of the overall mass and heat fluxes to be zero, and multiplying by C_p/g, where g is gravity, the following:

$$\frac{\partial H_c}{\partial t} = -\frac{C_p}{g}(\boldsymbol{v}_e \Delta p_1)\nabla T_1 - \frac{C_p}{g}\left(T_1 \sum_{k=2}^{N} \frac{\partial \Delta p_k}{\partial t} - \sum_{k=2}^{N} T_k \frac{\partial \Delta p_k}{\partial t}\right) - \frac{C_p}{g}\left\{(\boldsymbol{v}_r \Delta p_1)\cdot\nabla T_1 + \sum_{k=2}^{N}[(\boldsymbol{v}_k \Delta p_k)\cdot\nabla T_k]\right\}, \quad (9)$$

may be formulated. This equation is analogous to (5), except that no assumption has been made about the reference temperature of the compensatory flow. Thus the first term represents heat content change caused by horizontal Ekman transport, and the last term represents the advective heat content change brought about by fluid motion independent of the Ekman flow. Term 2 on the right-hand side represents the Ekman pumping. However, it also incorporates any other divergent flow in the water column. If water enters the water column in layer 2, say, and an equal amount leaves from layer 3, then the heat content change caused by this process will also be included in term 2. The main constituent of the non-Ekman flow should be the (nondivergent) geostrophic flow. However, there are motions that are independent of the Ekman flow but are divergent. These divergences cannot be separated from the compensatory divergent flow, and for this reason, this term can only represent an estimate of the heat content change due to Ekman pumping in the model and should therefore be viewed cautiously.

The annual average of term 2 is shown in Figure 15a, and the monthly zonal average is shown in Figure 15b. As can be seen from these figures, there is a qualitative similarity to the diagnostically calculated heat content changes shown in Figures 9b, 14a, 14b, and 12d, with zero lines being closely matched and the pattern of warming and cooling being the same. The western boundary in the annual average is very different from the diagnostic results, presumably because of the divergences eluded to above. Unfortunately, the figures do not permit an inversion to reveal an equivalent reference temperature for Figures 15a and 15b, as the presence of the divergences due to other motion forces significant errors. That is, T_{ref} cannot be accurately reproduced by the expression,

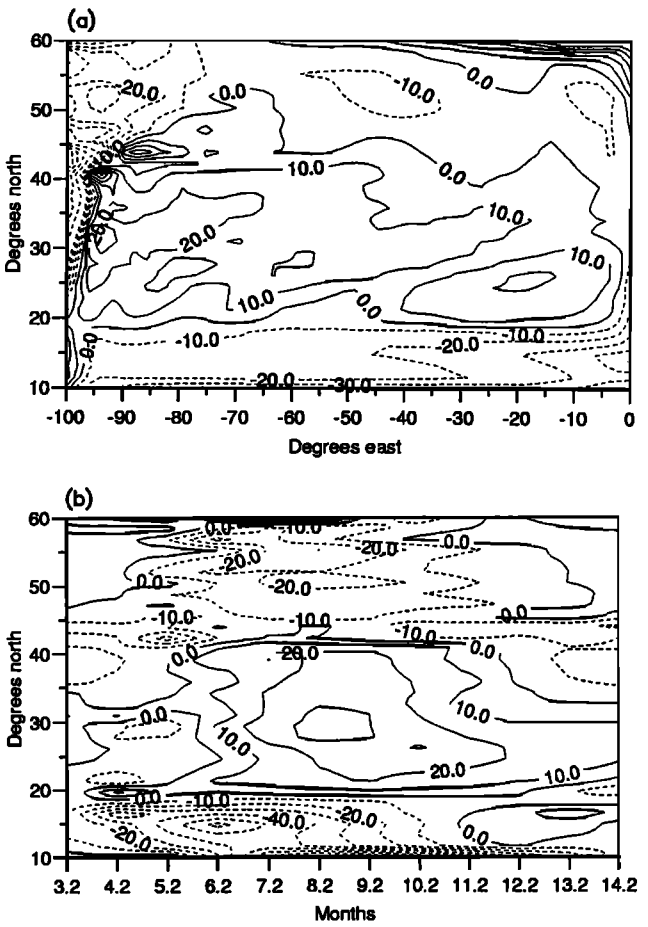

Figure 15. On-line heat content change due to Ekman pumping, (a) annually averaged, contours every 10 W/m^2 between $\pm$50 W/m^2 and every 50 W/m^2 beyond $\pm$50 with a zonal 1-2-1 filter applied, and (b) monthly zonal average (W/m^2).

$$T_{\text{ref}} = \frac{\sum_{k=2}^{N} T_k \partial \Delta p_k/\partial t}{\sum_{k=2}^{N} \partial \Delta p_k/\partial t}, \quad (10)$$

if $\partial \Delta p_k/\partial t$ is allowed to be negative for some k. This problem is exaggerated where the lines of zero Ekman pumping should be, as any slight errors become greatly magnified in these regions. However, though an accurate inversion is not possible, an informal visual comparison with Figures 9b, 14a, 14b, and 12d is feasible and suggests that the model compensatory flow is in the vicinity of the upper thermocline.

The question of the depth of the compensatory flow is also pertinent to the details of oceanic heat transport. It has been pointed out that, though the magnitude of the total heat transport remains unaffected by the precise definition of the Ekman process, the relative effects of the Ekman and non-Ekman contributions to the oceanic heat transport are entirely dependent on this definition [*Bryden et al.*, 1991; *Böning and Herrmann*, 1994]. As the Ekman contribution reflects the direct role of the wind stress, it remains an important but unanswered question as to what is this appropriate

reference depth. Successfully answering this question will result in greater knowledge of the effects on both the heat budget and on oceanic heat transport of any potential future changes to the wind stress field.

6.3. Zonal Averages

The seasonal heat balance is somewhat different from the annual one, as heat storage is no longer negligible. Indeed, Figures 12a–12e demonstrate that, to first order, the seasonal balance in the model is between the surface heating and the change in heat storage, as argued previously by *Gill and Niiler* [1973] and shown by *Sarmiento* [1986] but in contrast to the results of *Lamb and Bunker* [1982]. Not only is the magnitude of the surface fluxes far greater than the magnitude of any of the transport terms, but also the seasonal cycle is far more pronounced. What cycle there is in the transport terms is controlled by the Ekman terms, in particular, the Ekman pumping, which, in turn, are governed by the seasonal cycle of the winds and the degree of upper ocean stratification.

Figure 16 shows the monthly meridional heat transport in the model. Despite the domain not incorporating the equatorial regions to any great extent, it may be seen that there is still a seasonal cycle throughout the bulk of the subtropical gyre. *Böning and Herrmann* [1994] produced similar figures using a 1/3° resolution model for the region 15°S–65°N with two different wind stress fields. Qualitatively, their results are highly comparable to Figure 16, although the magnitude of the heat transport is somewhat less in this modeling study. *Sarmiento* [1986] also produced a plot of the monthly meridional heat transport, with the seasonal variation in the subtropics being no greater than that shown here. This qualitative similarity suggests that the intense cycle in the heat balance in the tropics is a relatively self-contained event, being constrained by the peculiar nature of the equatorial dynamics rather than directly influencing the seasonal cycle of the extratropical regions.

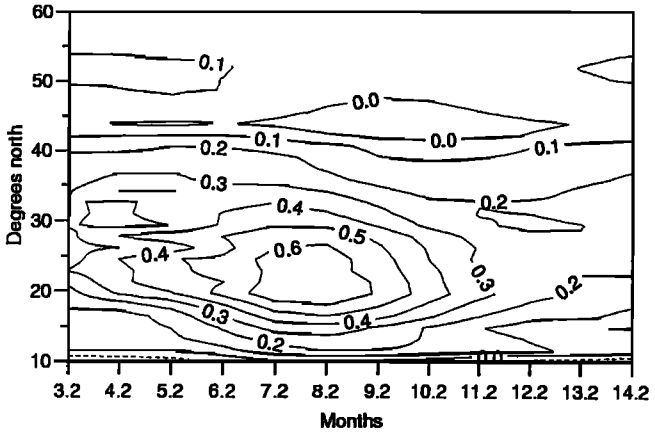

Figure 16. Monthly meridional heat transport (petawatts).

In the light of the zonally averaged results shown above (Figures 12a–12e), Figure 16 also strengthens the implication that it is the Ekman terms which are responsible for setting the seasonal cycle of advective heating within the extratropical North Atlantic.

7. Conclusions

Both annual and zonally averaged seasonal heat budget results have been obtained using an idealized isopycnic model approximating the North Atlantic. The experiment has been performed at a time of little net surface heating.

In the model North Atlantic, different regions have contrasting heat balances. Ekman pumping is crucial to the thermodynamics of the subtropical gyre, where the annually averaged surface forcing is small, but it is of little consequence in the subpolar gyre. There the non-Ekman advection becomes important, supplying heat that is lost to the atmosphere throughout the winter. Some heat is also lost by the southward transfer of water in the Ekman layer across the North Atlantic Current, while a little heat is gained through diffusive processes. To the south of the domain, heat gain from surface forcing and Ekman transport is balanced by Ekman suction. Different balances exist on shorter temporal scales, with surface forcing dominating everything seasonally but not necessarily annually.

Ekman processes have been examined, the results of these having been obtained both diagnostically using the model-produced temperature field and on-line. Both Ekman transport and Ekman pumping are seen to be important to the heat budget, Ekman pumping particularly so. Indeed, in the subtropical gyre, Ekman pumping becomes the dominant term in the annual heat budget and is seen to play a crucial role in the subduction process taking place in the subtropical gyre. These results complement the work of *Marshall et al.* [1993] and *Marshall and Marshall* [1995], who came to similar conclusions based on observational studies and theoretical considerations. In particular, the effects of Ekman pumping help control the location of the line of net zero buoyancy flux to the mixed layer [*Marshall et al.*, 1993; *Paillet and Arhan*, 1996], which may be instrumental in setting the water properties of the North Atlantic thermocline. Any changes in the distribution of wind stress in the subtropical gyre will affect the extent of Ekman pumping and, through this, the position of the line of net zero buoyancy flux to the mixed layer. Thus wind stress not only contributes to the ocean circulation but also can be seen to play a fundamental role in the ocean heat balance and then the climate system.

A note of caution needs to be added, though. The restricted domain and lack of inflow at the boundary mean that there is a large amount of heat that is not being transported through the domain. As the wind stress is independent of this and the temperature fields seem reasonable, the actual Ekman results should be little af-

fected by this limitation. However, the non-Ekman advection will not be fully captured in the present model configuration, most noticeably in the Gulf Stream region. Thus the results presented here can have only a certain degree of trustworthiness. Quantitatively, for example, the seasonal results are somewhat different from, say, the surface forcing of *Böning and Herrmann* [1994] or the heat transport divergence of *Sarmiento* [1986].

Similarly, the detail of the effects of Ekman pumping is uncertain, as the exact depth and, pertinently, the exact temperature, of the Ekman compensatory flow are unknown. This work has concentrated on the assumption of a compensatory flow in the thermocline, although the modeling tentatively suggests that the response may be higher in the water column than that. Even with a compensatory flow in the upper thermocline, though, the Ekman pumping is still an important factor in the heat budget of the subtropical gyre. It is also plausible that the compensatory flow is much deeper, in which case, the effects become greater. This dependence on the depth of the compensatory flow is suggested in Figure 8, as the term shown needs only to be multiplied by a constant factor and the temperature difference between the Ekman layer and the compensatory flow to obtain the heat content change caused by the Ekman pumping.

The Ekman transport and Ekman pumping results display seasonal cycles. Although this is not unexpected, given the seasonal cycle of the wind stress, it is interesting to note that, in the Ekman pumping results, the degree of stratification of the upper ocean appears to be more influential than the magnitude of the gradient in wind stress. In general, the seasonal amplitudes of the Ekman terms are far less than that of the surface forcing but are significantly more than that of either geostrophic advection or diffusion. The seasonal cycle of the heat content change caused by the transport of heat within the model ocean is therefore largely determined by the seasonal cycle of the Ekman terms.

The modeling has been carried out using a number of simplifications in order to ease understanding of the results and to reduce computing time. As noted above, a regional heat budget study is limited by exclusion of the exterior domain, and this work could therefore be taken forward by either extending the domain to incorporate the more northern reaches of the Atlantic and the equatorial regions or utilizing more sophisticated boundary conditions that allow more realistic heat flow. The inclusion of this heat flow should ensure a more realistic thermohaline overturning, which would be likely to significantly increase the heat flowing through the Gulf Stream. Similarly, the 2° resolution restricts the velocities achievable in the model and passes some of the advective responsibility to the diffusive terms. An eddy-resolving model would have the virtue of more realistically partitioning the advective contribution to the heat budget between mean and eddy terms.

The questions about the depth of the compensatory flow could also be examined more thoroughly with an increased vertical resolution, particularly in the mixed layer. During the winter months the complex processes taking place near the top of the ocean are somewhat smoothed over with the present model configuration. Some hybrid model that allowed the mixed layer to be subdivided might facilitate a better understanding of the compensatory flow, particularly if the Ekman layer could be explicitly represented.

Nevertheless, despite these shortcomings, qualitatively, the overall heat budget analysis is similar to that of early work. The seasonal picture is dominated by the surface fluxes in the extratropical regions, as previously shown by *Sarmiento* [1986] and *Böning and Herrmann* [1994] with models covering larger domains and, in the case of Böning and Herrmann, significantly finer resolution. Ekman pumping, even with a relatively low wind stress, is shown to be an important term in the region of subtropical subduction, as was suggested by *Marshall et al.* [1993], *Marshall and Marshall* [1995], and *Paillet and Arhan* [1996].

Acknowledgments. The authors would like to express their thanks to Ric Williams for productive discussions and insight on Ekman theory and to Adrian New and the James Rennell Division of the Southampton Oceanography Centre for supplying computer time. In addition, the paper was improved by comments from anonymous reviewers. In the period in which this work was carried out, I.J. was supported by a grant from the Natural Environment Research Council of the United Kingdom.

References

Bathén, K. H., Heat storage and advection in the North Pacific Ocean, *J. Geophys. Res., 76,* 676–687, 1971.

Bleck, R., H. P. Hanson, D. Hu, and E. B. Kraus, Mixed layer-thermocline interaction in a three-dimensional isopycnic coordinate model, *J. Phys. Oceanogr., 19,* 1417–1439, 1989.

Bleck, R., C. Rooth, D. Hu, and L. T. Smith, Salinity-driven thermocline transients in a wind- and thermohaline-forced isopycnic coordinate model of the North Atlantic, *J. Phys. Oceanogr., 22,* 1486–1505, 1992.

Böning, C. W., and P. Herrmann, Annual cycle of poleward heat transport in the ocean: Results from high-resolution modeling of the North and Equatorial Atlantic, *J. Phys. Oceanogr., 24,* 91–107, 1994.

Bryden, H. L., D. H. Roemmich, and J. A. Church, Ocean heat transport across 24°N in the Pacific, *Deep Sea Res., Part A, 38,* 297-324, 1991.

Cai, W., R. J. Greatbatch, and S. Zhang, Interdecadal variability in an ocean model driven by a small, zonal redistribution of the surface buoyancy flux, *J. Phys. Oceanogr., 25,* 1998–2010, 1995.

Cox, M. D., An eddy resloving numerical model of the ventilated thermocline, *J. Phys. Oceanogr., 15,* 1312–1324, 1985.

Gent, P. R., and J. C. McWilliams, Isopycnal mixing in

ocean circulation models, *J. Phys. Oceanogr., 20,* 150–155, 1990.

Gill, A. E., and P. P. Niiler, The theory of the seasonal variability in the ocean, *Deep Sea Res., 20,* 141–177, 1973.

Hall, M. M., and H. L. Bryden, Direct estimates and mechanisms of ocean heat transport, *Deep Sea Res., Part A, 29,* 339–359, 1982.

Hellermann, S., and M. Rosenstein, Normal monthly wind stress over the World Ocean with error estimates, *J. Phys. Oceanogr., 13,* 1093–1104, 1983.

Isemer, H.-J., and L. Hasse, *The Bunker Climate Atlas of the North Atlantic Ocean,* vol. 1, *Observations,* 218 pp., Springer-Verlag, New York, 1985.

Isemer, H.-J., J. Willebrand, and L. Hasse, Fine adjustment of large scale air-sea energy flux parameterizations by direct estimates of ocean heat transport, *J. Clim., 2,* 1173–1184, 1989.

Kraus, E. B., and J. S. Turner, A one-dimensional model of the seasonal thermocline, II, The general theory and its consequences, *Tellus, 19,* 98–106, 1967.

Lamb, P. J., and A. F. Bunker, The annual march of the heat budget of the North and Tropical Atlantic Oceans, *J. Phys. Oceanogr., 12,* 1388–1410, 1982.

Levitus, S., Climatological atlas of the world ocean, *NOAA Prof. Pap., 13,* 173 pp., U. S. Govt. Print. Office, Washington, D. C., 1982.

Marshall, D., and J. Marshall, On the thermodynamics of subduction, *J. Phys. Oceanogr., 25,* 138–151, 1995.

Marshall, J. C., A. J. Nurser, and R. G. Williams, Inferring the subduction rate and period over the North Atlantic, *J. Phys. Oceanogr., 23,* 1315–1329, 1993.

McCulloch, M. E., Seasonal heat and freshwater fluxes in the Northeast Atlantic, Ph.D. thesis, 128 pp., Liverpool Univ., Liverpool, England, 1995.

New, A. L., and R. Bleck, An isopycnic model study of the North Atlantic, II, Interdecadal variability of the subtropical gyre, *J. Phys. Oceanogr., 25,* 2700–2714, 1995.

New, A. L., R. Bleck, Y. Jia, R. Marsh, M. Huddleston, and S. Barnard, An isopycnic model study of the North Atlantic, I, Model experiment, *J. Phys. Oceanogr., 25,* 2667–2699, 1995.

Nurser, A. J. G., and J. C. Marshall, On the relationship between subduction rates and diabatic forcing of the mixed layer, *J. Phys. Oceanogr., 21,* 1793–1802, 1991.

Paillet, J., and M. Arhan, Shallow pycnoclines and mode water subduction in the Eastern North-Atlantic, *J. Phys. Oceanogr., 26,* 96–114, 1996.

Rind, D., D. Peteet, W. S. Broecker, A. McIntyre, and W. Ruddiman, The impact of cold North Atlantic sea surface temperatures on climate: Implications for the Younger Dryas cooling (11–10k.), *Clim. Dyn., 1,* 3–33, 1986.

Sarmiento, J. L., On the North and tropical Atlantic heat balance, *J. Geophys. Res., 91,* 11,677–11,689, 1986.

Schmitt, R. W., P. S. Bogden, and C. E. Dorman, Evaporation minus precipitation and density fluxes for the North Atlantic, *J. Phys. Oceanogr., 19,* 1208–1221, 1989.

Wang, X., P. H. Stone, and J. Marotzke, Poleward heat transport in a barotropic ocean model, *J. Phys. Oceanogr., 25,* 256–265, 1995.

Woodruff, S. D., R. J. Slutz, R. L. Jenne, and P. M. Steurer, A comprehensive ocean-atmosphere dataset, *Bull. Am. Meteorol. Soc., 68,* 1239–1250, 1987.

I. Jones, Environment Centre, Leeds University, Leeds LS2 9JT, England, United Kingdom. (ian@lec.leeds.ac.uk)

H. Leach, Oceanography Laboratories, Liverpool University, Liverpool L69 3BX, England, United Kingdom.

(Received September 23, 1997; revised September 25, 1998; accepted October 9, 1998.)